COBEM 2023 27TH INTERNATIONAL CONGRESS OF MECHANICAL ENGENEERING

ABCM Brazilian Society of Mechanical Sciences and Engineering
27th ABCM International Congress of Mechanical Engineering
December 04-08, 2023, Florianópolis-SC, Brazil

COB-2023-1003
COMPARATIVE STUDY OF HAPTIC INTERFACES WITH PARALLEL AND SERIAL KINEMATIC CONFIGURATION

Liz Carolina Jaber Costato
Walter de Britto Vidal Filho
Universidade de Brasília
liz.jaber@aluno.unb.br, wbritto@unb.br

Abstract. *Haptic interfaces are computer devices used for inputting and outputting data, providing users with threedimensional hand movement and force feedback. Originally developed for gaming, they are now utilized in the teleoperation of robotic arms and simulators. Historically, teleoperation involved mechanical telemanipulators, in which the user's movements were transmitted to a slave manipulator through bars and cables. With advancements in digital electronics, haptic interfaces nowadays can act as the master manipulator, even with different structural configurations than the slave manipulator. Two simplified 2D configurations, parallel and serial, were studied for haptic interface development. The cable-activated closed kinematic chain configuration was chosen for its low movement inertia, while the articulated configuration was selected for the serial configuration. Two prototypes were built and tested, employing Python and different potentiometers as position sensors. The results include descriptions of the tests, assemblies, advantages, disadvantages, functionality, and costs associated with each prototype. These results indicated that the series prototype studied has more advantages than the parallel one, and, therefore, a 3D prototype with this configuration should be followed.*

Keywords: *haptic, comparative study, parallel configuration, serial configuration, structure*

1. INTRODUCTION

The first master-slave devices for teleoperation of robotic manipulators (Fig. 1) were the ancestors of the current haptic interfaces used in simulation and teleoperation. They were purely mechanical devices initially employed for handling radioactive materials (Goertz *et al.*, 1961). These devices evolved into electromechanical systems and later into electronically controlled systems. Haptic interfaces are recent developments and emerged for interaction with computer systems, primarily in virtual simulations. Haptic devices are equipment that enables immersive human-machine interaction. By interacting with the user, the device captures their position and movements and provides force feedback resulting from the interaction with the virtual environment, giving the user a sense of touch (Khan, 2008).

The use of haptic devices is diverse, particularly due to their precision and the ability to control equipment remotely. For example, they can be applied in teleoperation contexts for equipment in dangerous or unhealthy environments, aiming to ensure the safety of workers and the integrity of the equipment (Campos, 2019). In the medical field, they find applications in simulators for surgical training, as well as in remote surgeries that require high precision (Morrell *et al.*, 2021).

This study aims to compare two 2D prototypes, analyzing two possible structures, to obtain mechanical design parameters for a haptic interface to be used in a surgical simulator. Both prototypes should be able to capture the position of the user's hand in a specific workspace: a square with sides of 200mm, as shown in Fig. 4a. Selected points in space will be measured by both devices, and the analysis of associated errors will be performed for subsequent comparison. The prototypes currently do not have the haptic function of force feedback, but only capture the position of interest.

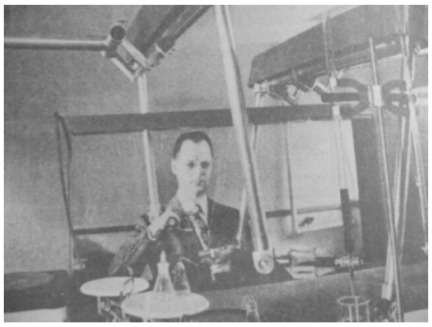

Figure 1: Mechanical master-slave manipulator (Goertz *et al.*, 1961).

2. BACKGROUND KNOWLEDGE

Haptic devices can be classified into ground-based devices, which connect the end effector to a base or the ground, or body-based devices, where the user wears or is covered by the device. Furthermore, there is a classification based on the type of mechanism, whether it is parallel or series, and according to the control system, which can be impedance or admittance-based (Khan, 2008). The focus of this study is to compare two two-degree-of-freedom devices, both ground-based and impedance control devices (Khan, 2008). The two devices vary in terms of structure, with one being a series and the other a parallel mechanism.

The configuration of links and joints can divide manipulators into series or parallel devices. The series configuration, also known as an open kinematic chain, refers to devices where the joints are connected in series until the end effector (Figs. 2a and 2b) (Silva, 2014). In this study, the articulated configuration with two revolute joints (Carrara, 2015) will be analyzed (Fig. 2b). On the other hand, in parallel mechanisms, also known as closed kinematic chains, the multiple joints form at least one closed loop, with only a few of their joints being actuated (Silva, 2014). Although they have a reduced workspace or volume, these mechanisms generally offer high precision (Silva, 2014). Furthermore, they are classified based on the number of degrees of freedom they possess (Figs. 2c and 2d).

Within these categories, there is a specific parallel configuration that uses flexible cables to connect the end effector, known as Cable-Driven Parallel Robots (CDPRs). This approach offers several advantages over conventional rigid cable options, such as a larger workspace and lower fabrication cost (Qian *et al.*, 2018). In this study, a system with flexible cables and two degrees of freedom will be proposed for subsequent comparison with the articulated series configuration.

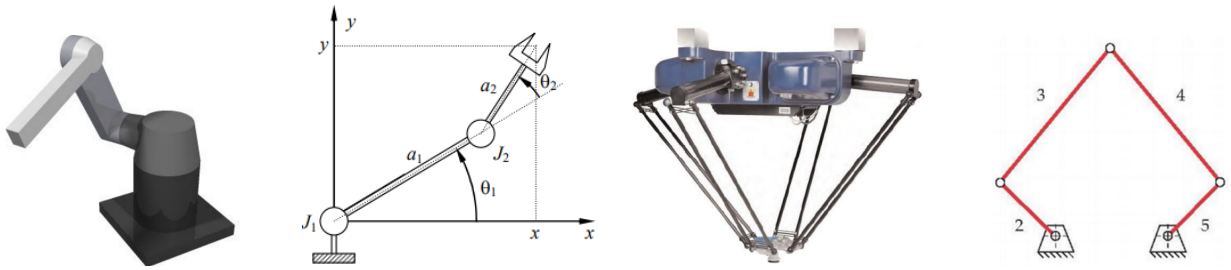

(a) Serial configuration 3D. (b) Serial configuration 2D. (c) Parallel configuration 3D. (d) Parallel configuration 2D.

Figure 2: Examples of parallel and articulated configurations (Carrara, 2015) (Silva, 2014).

3. METHODOLOGY

3.1 Sensor Selection and Associated Error Determination

The positioning of a user's hand is determined by the location of the end effector in the two proposed prototypes. Therefore, position sensors are required. The main sensors used in haptic mechanisms are encoders and potentiometers. The process of selecting the sensor involves considering the desired precision, the device size, the need for electronic boards, and also the cost. Potentiometers were chosen for study due to their precision and low cost. Additionally, an encoder model was also analyzed due to its precision and frequency of use in similar applications (Forsslund *et al.*, 2015; Martin and Hillier, 2009). Ultimately, potentiometers were chosen as position sensors for both studied mechanisms, considering their low cost, ease of use, and sufficient precision for the desired objective. The selected potentiometer models were a single-turn potentiometer with a total resistance of 5kΩ and a 10-turn potentiometer with a total resistance of 10kΩ.

Tests were conducted within the operating ranges of the selected sensors, comparing the obtained readings with the actual angular variations in the potentiometers. An Arduino Uno was used to read the sensors, with a 5V power supply connected to the potentiometer terminals. The actual angular variation was measured using a protractor with 1º increments. It is important to notice that, because the Arduino's analog readings provide integer values ranging from 0 to 1023, there is an associated error with these readings. To cover the entire operating range of the sensors, an expected precision of approximately $350°/1024 = 0.3418°$ was considered for the simple potentiometer, and $3590°/1024 = 3.5059°$ for the multi-turn potentiometer, taking into account the analog-to-digital conversion performed by the Arduino. By performing the proposed tests, considering the uncertainties associated with the sensor and the protractor, as well as Arduino's analog-to-digital conversion, average errors of 1.8621º and 5.1473º, and maximum errors of 5.8285º and 29.2982º were obtained for the simple potentiometer and the multi-turn potentiometer, respectively. However, when disregarding the last turn of the multi-turn potentiometer, which presented a significantly higher associated error (as shown in Fig. 3), the average error was 4.6177º, and the maximum error was 9.7570º for this sensor.

Figures 3a, 3b, and 3c illustrate the results obtained in the experiments. It is important to note that these values can be converted to millimeters within the workspace, depending on how the sensors are used. Therefore, the associated error in

millimeters will be further explained in conjunction with the presentation of the prototypes in the upcoming sections.

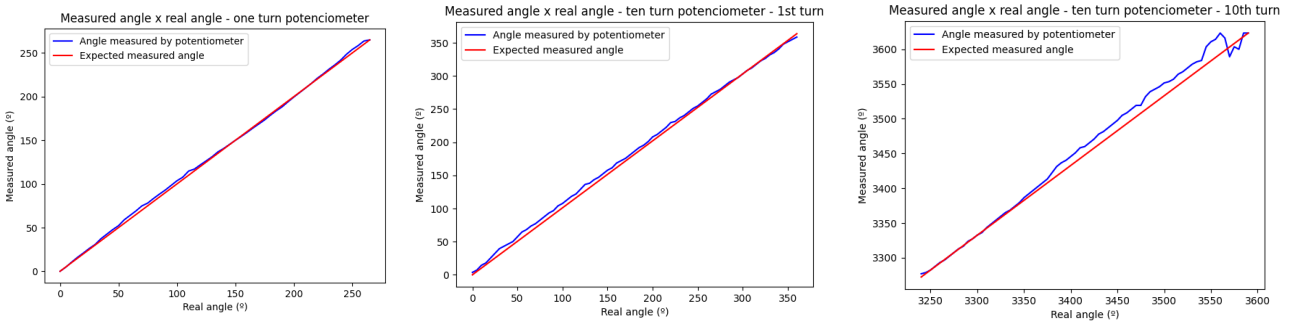

(a) Single-turn potentiometer. (b) Multi-turn potentiometer, in the first turn. (c) Multi-turn potentiometer, in the tenth turn.

Figure 3: Tests with the chosen potentiometers, within their respective operating ranges.

3.2 Mathematical modeling

According to Quian et al. (2018), parallel cable-driven robots can be classified into three types, depending on the relationship between the number of degrees of freedom, n, and the number of cables, m: underconstrained if n+1 > m, fully constrained if n+1 = m, or redundantly constrained if n+1 < m. When underconstrained, the robot's position can exhibit significant fluctuations, whereas when redundantly constrained, cable conflicts may arise, preventing access to certain positions in the workspace. Therefore, for the 2D prototype with two degrees of freedom, it was decided to use 3 cables, with each cable associated with a position sensor. The chosen sensor was the 10-turn potentiometer. Figures 4b and 4c depict the schematics of the proposed prototypes, one with cables and three sensors, and the other with two bars and two sensors.

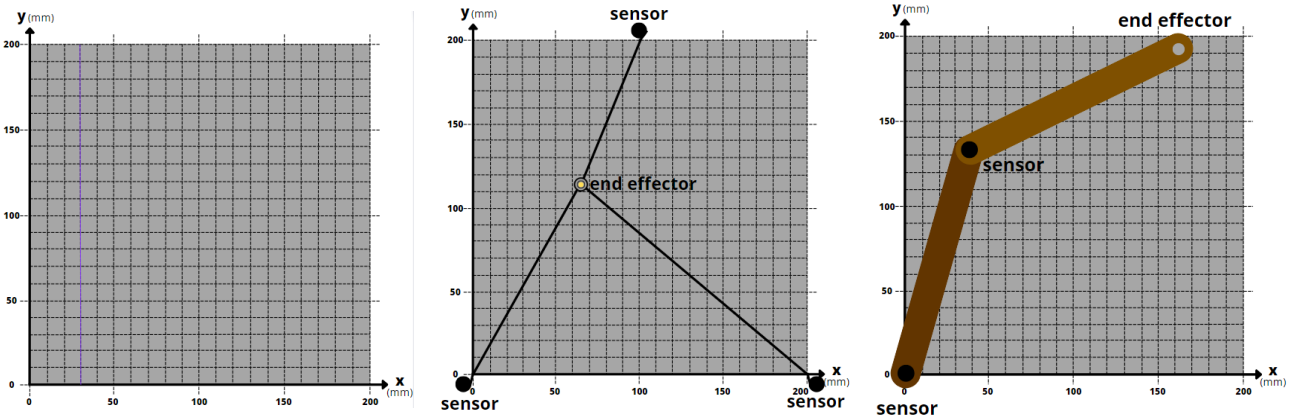

(a) Workspace for both devices. (b) Schematic of parallel mechanism. (c) Schematic of serial mechanism.

Figure 4: Proposed workspace and configurations of the prototypes.

The direct kinematics modeling of position for both prototypes was analyzed. In the parallel prototype, as the potentiometer rotates when the cable is stretched, the reading of the rotated angle is proportional to the distance from the end of the cable (end effector position) to the sensor. Thus, each reading provides a circumference of possibilities for the location of the end effector, with the potentiometer being the center of the circumference. The position in the cable configuration can then be modeled by the intersection of the circumferences corresponding to the three cables. Using the variables defined in Fig. 5, the solution of the system of Equations 1, 2 and 3 determines the coordinates (x, y) of the end effector, in mm.

$$x^2 + y^2 = r_1^2 \tag{1}$$

$$(x - 200)^2 + y^2 = r_2^2 \tag{2}$$

$$(x - 100)^2 + (y - 200)^2 = r_3^2 \tag{3}$$

To address the potential errors associated with the sensor readings, an approach was developed that considers four study cases to be analyzed. These cases are as follows:

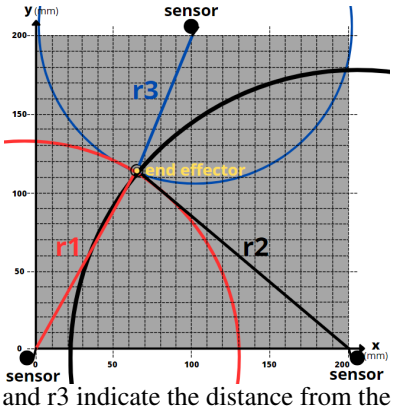

Figure 5: The radius r1, r2, and r3 indicate the distance from the end effector to each sensor.

• The first case corresponds to the situation where the circumferences intersect at a single point, which is considered the ideal case. In this scenario, the intersection point coincides with the point of interest, as illustrated in Fig. 6a.

• The second case occurs when the three circumferences intersect but do not share any common points. In this situation, it is estimated that the desired point can be approximated by the intersection of the lines formed by the circumference intersections, as depicted in Fig. 6b.

• The third case is characterized by the intersection of only two pairs of circumferences. In this case, it is also considered that the desired point can be approximated by the intersection of the lines formed by the corresponding intersections, as demonstrated in Fig. 6c.

• Finally, there is the case where no circumference intersects with another. In this scenario, it is assumed that all the readings were smaller than they should be, due to the associated sensor error. Therefore, an arbitrary distance d is added to all the readings until one of the previous cases occurs.

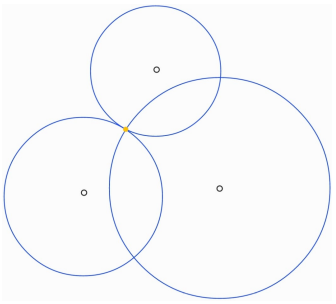

(a) Case in which they intersect at one point.

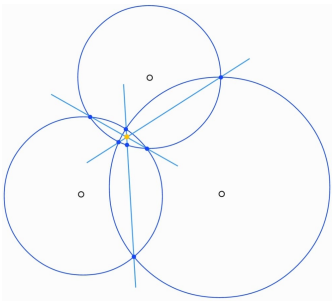

(b) Case in which all intersect, but without common points.

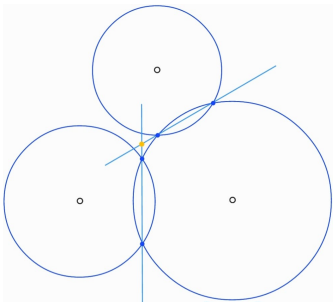

(c) Case in which only two pairs intersect.

Figure 6: Possibilities of intersection of the three circumferences.

In the case of the series mechanism, the modeling is obtained through geometry. Equations 4 and 5 demonstrate how to obtain the desired coordinates (x, y) (Carrara, 2015), where a_1, a_2, θ_1, and θ_2 are defined in Fig. 8b.

$$x = a_1 cos(\theta_1) + a_2 cos(\theta_1 + \theta_2) \tag{4}$$

$$y = a_1 sin(\theta_1) + a_2 sin(\theta_1 + \theta_2), \tag{5}$$

3.3 Force Feedback

It is important to consider the possibility of using these systems with haptic feedback, which involves providing force feedback in addition to obtaining the position of the end effector. One viable approach would be to add a motor to each sensor in both prototypes, applying traction to the cables in the parallel mechanism or torque to the joints in the series mechanism.

By implementing this approach, it would be possible to provide force feedback in all directions and points of the workspace using the series mechanism. However, in the case of the parallel mechanism, the ability to apply force in all directions would be limited to the highlighted region in Fig. 7a. In other areas of the workspace, only forces in specific directions could be exerted, as shown in Fig. 7b.

With the angles and forces defined in Fig. 8a, the forces to be applied to the cables of the parallel prototype, in order to provide a haptic response formed by the components F_x and F_y, can be obtained using Equations 6 and 7, respectively.

(a) Area where force could be applied.

(b) Possible forces with the end effector in different positions.

Figure 7: Area and possible forces in the parallel mechanism.

However, since there are three unknown forces, F_1, F_2, and F_3, and only two equations, one of the forces must be arbitrarily chosen to determine the others. The angles θ_1, θ_2 and θ_3 of this mechanism are obtained by the equations 8, 9 and 10. Furthermore, it is worth noting that the relationship between the forces F_1, F_2, and F_3, and the torque applied by each motor is given by $\vec{T} = \vec{F}x\vec{R}$, where R is the radius of the shaft connecting the motor and the cable.

In the case of the series prototype, with the angles and forces defined in Fig. 8b, the torques to be applied to the series prototype are calculated according to Equations 11 and 12. The angles θ_1 and θ_2 of this mechanism are obtained directly from the sensor readings. In both systems, if the intention is only to maintain the end effector in the position where the user left it, it is sufficient to set the components of force F (F_x and F_y) equal to zero. However, if force feedback is desired, F can be set to the desired force, then decomposed into (F_x and F_y), and the presented Equations can be applied.

$$F_x = \begin{cases} F_1 \cdot cos(\theta_1) - F_2 \cdot cos(\theta_2) - F_3 \cdot sin(\theta_3), \text{if } x < 10; \\ F_1 \cdot cos(\theta_1) - F_2 \cdot cos(\theta_2) + F_3 \cdot sin(\theta_3), \text{if } x \geq 10. \end{cases} \tag{6}$$

$$F_y = F_1 \cdot sin(\theta_1) + F_2 \cdot sin(\theta_2) - F_3 \cdot sin(\theta_3) \tag{7}$$

$$\theta_1 = arctan(\frac{y}{x}) \tag{8}$$

$$\theta_2 = arctan(\frac{y}{20 - x}) \tag{9}$$

$$\theta_3 = arctan(\frac{|10 - x|}{20 - y}) \tag{10}$$

$$T_2 = -F_y \cdot a_2 \cdot cos(\theta_1 + \theta_2) - F_x \cdot a_2 \cdot sin(\theta_1 + \theta_2) \tag{11}$$

$$T_1 = T_2 - F_y \cdot a_1 \cdot cos(\theta_1) - F_x \cdot a_1 \cdot sin(\theta_1) \tag{12}$$

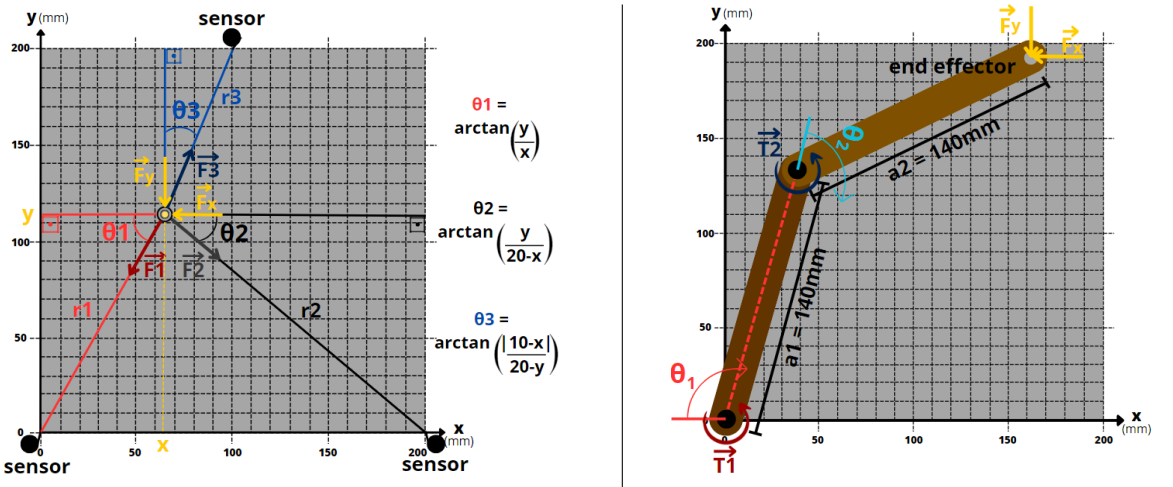

(a) Angles and forces adopted in the parallel prototype.

(b) Angles and forces adopted in the series prototype.

Figure 8: Reference angles for calculating the applied forces.

3.4 Parallel mechanism prototype

The final prototype obtained for the 2D parallel mechanism can be observed in Fig. 9. The design decisions for this system will be further explained.

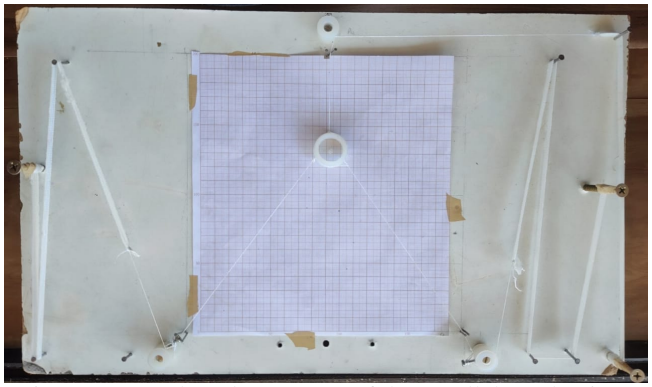

Figure 9: Developed prototype of the parallel mechanism.

In order that the movement of the wire also rotates the potentiometer, allowing for the measurement of its displacement, a pulley was designed as presented in Figs. 10a and 10b. The pulley is made of Nyln material and is fixed to the potentiometer shaft with a screw. The pulley's radius was defined to ensure that the entire workspace can be fully monitored. For this purpose, it was considered that the longest length to be measured is the diagonal of the area in Fig. 4a, which is equal to $200 \cdot \sqrt{2}$ mm. Additionally, tests conducted with the sensor revealed a significant error in the last turn of the potentiometer. Therefore, it was decided to use only the first 9 possible turns. Considering 9 rotations of the potentiometer shaft, Equation 13 was used.

$$2 \cdot \pi \cdot R \cdot 9 = 200 \cdot \sqrt{2}, \tag{13}$$

where the left-hand side of the equation corresponds to the total circumference length of the pulley with radius R, in mm, rotating the desired 9 turns of the potentiometer, and the right-hand side corresponds to the desired total length. From this equation, it was determined that the pulley radius, R, should be 5mm.

A device was developed to ensure that the cables connected to each potentiometer intersect at the same point of interest, tangentially, as shown in Fig. 10c. The designed and produced part can be better visualized in Fig. 10d.

(a) Pulley designed with a groove for wire passage.

(b) Pulley coupled to the shaft of the 10-turn potentiometer.

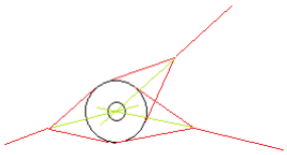

(c) Strategy for cables to converge to a common point.

(d) Visualization of grooves intended to each cable.

Figure 10: Components designed for the parallel prototype.

3.4.1 Theoretical Error of the Prototype

Considering the pulley positioned on the sensor's shaft with a radius of 5mm, the length of the wire stretched from the pulley is $2 \cdot \pi \cdot 5 \cdot \Delta\theta$, where $\Delta\theta$ is the angular variation of the sensor. As mentioned in section 3.1, the maximum error of the chosen sensor is 9.7570º. Therefore, in millimeters, the maximum error is

$$2 \cdot \pi \cdot 5 \cdot \frac{9.7570^\circ}{360^\circ} = 0.8515mm \tag{14}$$

3.5 Serial Mechanism Prototype

The serial mechanism was implemented as a planar Rotational-Revolute (RR) joint manipulator (Carrara, 2015). The final prototype can be observed in Fig. 11.

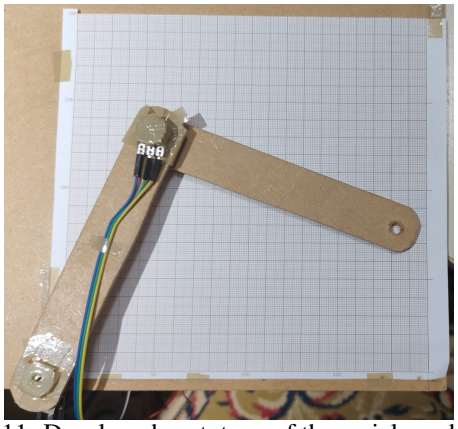

Figure 11: Developed prototype of the serial mechanism.

The linkages of the mechanism were constructed using MDF material, as well as the base on which the mechanism was mounted. For the two joints of the mechanism, simple potentiometers with a resistance of 5KΩ were chosen as sensors.

Single-turn potentiometers were chosen because by directly applying them to the linkages the error would be smaller compared to multi-turn potentiometers. Multi-turn sensors would only be advantageous if a gear reduction was implemented, but this option was not adopted in the project.

3.5.1 Theoretical Error of the Prototype

For the chosen configuration, the point of interest can be obtained from Equations 4 and 5, where a_1, θ_1, a_2, and θ_2 are defined according to the schematic presented in Fig. 4c. The links of the serial manipulator prototype have a length of 140mm.

Therefore, considering the maximum error of the simple potentiometer with one turn, which is 5.8285º, the maximum expected error in millimeters can be determined using the relationships given by Equations 15 and 16.

$$x = 140 \cdot [cos(5.8285^\circ) - cos(0^\circ)] + 140 \cdot [cos(5.8285^\circ) - cos(0^\circ)] + [cos(5.8285^\circ) - cos(0^\circ)] = 2.1713mm \quad (15)$$

$$x = 140 \cdot sin(95.8285^\circ - sin(90^\circ)) + 140 \cdot [sin(95.8285^\circ) - sin(90^\circ)] + [sin(95.8285^\circ) - sin(90^\circ)] = 2.1713mm \quad (16)$$

4. EXPERIMENTAL TESTS

Two Python programs were developed, one for each prototype to obtain the points measured by the system. The *pyfirmata* library was used to establish bidirectional communication with the Arduino, enabling command sending and data reading. In addition, the creation of an interactive graphical interface was performed using the *tkinter* library, allowing the user to intuitively visualize the workspace and track the current point of the system. This real-time visualization provides an immersive experience and facilitates the user's understanding of the system's operation.

Tests were performed with the points defined in Fig. 12a to determine the average error of each prototype distributed in the workspace (Fig. 4a). Furthermore, three analysis regions were defined to understand the behavior of the system's error. Regions 1, 2, and 3 in the workspace were established differently for each prototype according to the way the devices were constructed. Regions 1, 2 and 3 in Fig. 12b correspond to the parallel system and those in Fig. 12c to the serial system.

For each point of interest, the system underwent a measurement procedure in which three results were obtained. This procedure involved initially positioning the system at the desired point of interest, then randomly moving it to various positions in the workspace, and finally repositioning it back to the point of interest. This measurement cycle was repeated three times for each point of interest. After performing these measurements, the average absolute error was calculated for each point, considering the three repetitions. In addition, for each prototype, the mean of all the errors obtained was calculated, and the maximum error value was observed.

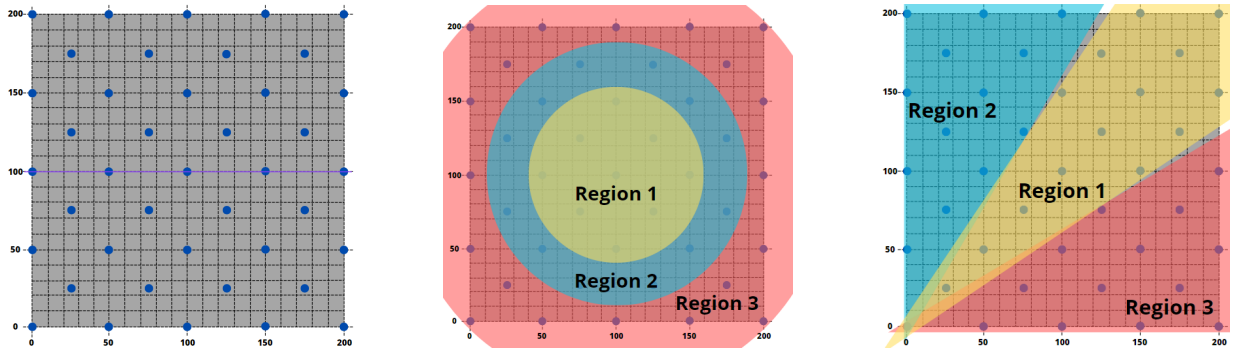

(a) Points for error analysis in both prototypes.

(b) Error analysis regions in the parallel device.

(c) Error analysis regions in the serial device.

Figure 12: Approach for error analysis.

5. RESULTS

5.1 Associated Error of the Constructed Prototypes

The data collection procedure described in Section 4using the Python programs communicating with the Arduino Uno that collects data from the prototypes. Figs. 13a and 13b show in blue the points in the workspace to which the system was taken three times. In red, the readings obtained from the three observations are displayed. There are proposed points in Fig. 12a that do not appear in blue in Figs. 13a and 13. This is due to physical limitations in the construction of the system that prevented the prototype from reaching those points of interest.

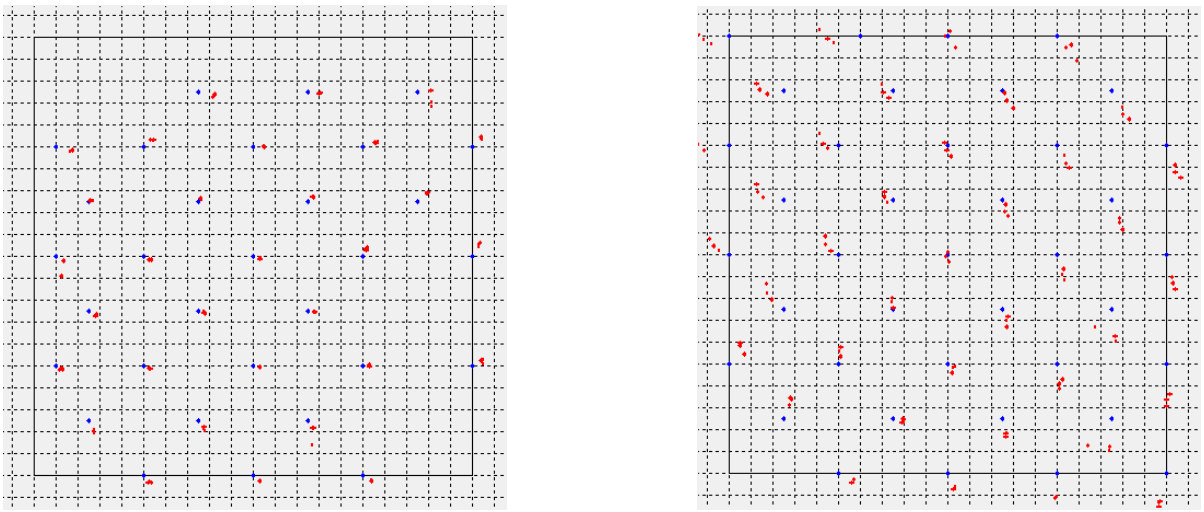

(a) Points obtained in the parallel prototype.

(b) Points obtained in the series prototype.

Figure 13: Errors associated with each prototype. The red dots correspond to the measurements and the blue dots to the reference position.

The average and maximum errors in each axis of the system for both prototypes can be obtained from these data. The results are presented in Tabs. 1 and 2. The analysis of average and maximum errors per region (defined in Figs. 12b and 12c) can be found in Tabs. 3 and 4.

Table 1: Average and maximum errors in the parallel mechanism.

	x (mm)	y (mm)
average error	1.95514	2.0310
maximum error	6.4203	8.3945

Table 2: Average and maximum errors in the series mechanism.

	x (mm)	y (mm)
average error	4.3422	5.8659
maximum error	16.1133	16.2960

It is evident that the parallel prototype exhibited smaller errors than the series prototype, both in terms of average and absolute values. This is mainly due to the use of a more accurate sensor, as well as the inclusion of redundancy in the

	Region 1		Region 2		Region 3	
	x (mm)	y (mm)	x (mm)	y (mm)	x (mm)	y (mm)
average error	1.1304	1.7410	2.5461	1.8822	2.0389	2.4170
maximum error	3.8470	3.8875	5.9957	8.3945	6.4203	6.5938

Table 3: Errors of the parallel mechanism by region of the workspace (Fig. 4a).

	Region 1		Region 2		Region 3	
	x (mm)	y (mm)	x (mm)	y (mm)	x (mm)	y (mm)
average error	2.6341	5.8635	7.5593	4.4622	2.83309	7.2720
maximum error	7.6682	12.2436	16.1133	11.6459	10.8460	16.2959

Table 4: Errors of the series mechanism by region of the workspace (Fig. 4a).

parallel mechanism, by using a third sensor.

It is also noticeable that, in both systems, Region 1 showed better performance, while Regions 2 and 3 had similar errors. In the parallel mechanism, this is because the error increases with the distance of the point of interest from the sensors. In other words, the central region, where the distances to all three sensors are similar and none is too far, exhibits lower errors compared to regions where the sensors are more distant from the point of interest

The division of regions was carried out to evaluate the influence of the sensor measuring θ_1 (defined in Fig. 8b) in the series system. It was observed that in areas where θ_1 has a lesser influence on the point of interest, i.e., when $cos(\theta_1)$ or $sin(\theta_1)$ approach zero, the calculations of the x or y coordinates (Equations 4 and 5, respectively) result in smaller errors. On the other hand, in areas where $cos(\theta_1)$ or $sin(\theta_1)$ approach 1, the error in the corresponding coordinate is larger. It was also observed that the measured range of θ_1 was larger than $90°$. Therefore, a recalibration of the relationship between the sensor reading and the measured angle, such that the total variation of θ_1 is $90°$, would result in a reduction of the obtained error.

The difference between the theoretical error for the parallel prototype, as given by Equation 14, and the observed error in Tab. 1, as well as the difference between the theoretical error for the series prototype, given by Equations 15 and 16, and the observed error in Tab. 2, is attributed to factors other than uncertainties related to the sensor and Arduino. These differences may be caused by inaccuracies in the construction of the prototype, such as misalignment, improper positioning, and component lengths. Additionally, the manual positioning of the systems at the point of interest can also introduce errors. Although a millimeter paper was used to assist in positioning the end effector at the test point, there can still be an error of up to 0.5 mm in this step.

5.2 Comparison between the constructed prototypes

In addition to the error, other criteria were used to compare the series mechanism and the parallel mechanism, such as cost, robustness, reach area, ease of reproduction, and ease of use.

Although the parallel prototype exhibited significantly lower average and maximum errors, the series mechanism proved superior in other factors. While the former utilized three sensors, the latter required only two. Additionally, the sensor used in the parallel prototype is more expensive than the one used in the series implementation. Therefore, in terms of cost, the series mechanism was more affordable.

However, it is important to highlight that for the desired workspace (Fig. 4a), positioning two potentiometers at the vertices of the square yields only one point of intersection of the circumferences formed by the distance between the point of interest and each sensor. Therefore, it is possible to determine the point of interest using only two sensors, eliminating the need for the third one. However, this approach results in the loss of redundancy provided by the third sensor, which means there will be no corrective indication for reading errors of the two potentiometers used. This potentially results in an increase in the obtained error. Additionally, the haptic feedback proposed in Section 3.3would not be possible.

Regarding the criterion of workspace, it can be observed in Figs. 13a and 13b that the series mechanism reached more points compared to the parallel mechanism. This is due to the difficulty of maneuvering the parallel end effector due to the tension of the used elastics. On the other hand, the series mechanism only missed two points: the origin, which is a limitation of the system itself, and the point x = 200mm and y = 200mm, which occurred due to an error in the size of the linkages that were small to reach that point

Due to the fragility of the cables and elastics used in the parallel prototype, the series mechanism is more robust. Furthermore, Furthermore, the serial configuration proved to be easier for manufacturing and for developing the program that obtains the point of interest from the prototype. Finally, due to the cables and elastics used, the parallel mechanism showed greater resistance to hand movements by the user compared to the series mechanism, making its use more challenging.

5.3 Proposed Improvements

Improvements can be made to both devices to enhance their identified limitations. In the parallel mechanism, in order to reduce resistance to movement, increase its workspace, and improve its robustness, the elastics used can be replaced with motors equipped with controllers. These motors would keep the system at the desired point while allowing movement when the system detects that the user wants to move the end effector. This system could also be programmed to provide force feedback to the user, functioning as a haptic device.

In the serial mechanism, a potential improvement involves replacing the single-turn potentiometer with a multi-turn potentiometer. Additionally implementing a reduction system using a set of pulleys to ensure that the angular displacement of the device's arms is smaller than that of the potentiometer. This would increase the sensor's precision by utilizing the full angular variation allowed by the multi-turn potentiometer, while monitoring the same workspace.

6. CONCLUSIONS

The present study conducted a comprehensive comparison between two 2D mechanisms, one in series configuration and the other in parallel configuration, aiming to evaluate their suitability for medical applications. Various criteria were considered, including error, cost, robustness, workspace, ease of replication, and ease of use. Although the parallel prototype exhibited significantly lower average and maximum errors, the series mechanism outperformed in other criteria, such as the use of fewer sensors and lower cost. The series mechanism also reached more points within the desired workspace and demonstrated higher robustness and ease of fabrication. Thus, the serial device proved to be more suitable to proceed with the development of a 3D haptic prototype, aiming at applications in teleoperation and surgical simulator

Both devices have potential for improvement. In the case of the parallel mechanism, the use of servo-controlled motors will be considered to replace the elastics. This would increase the workspace, reduce resistance to movement, and increase sturdiness, but the positioning accuracy results would be the same. For the series mechanism, it is recommended to replace the simple potentiometer with a multi-turn potentiometer and implement a reduction system using a set of pulleys. These improvements would enhance the sensor's precision, allowing for the full utilization of the potentiometer's angular range while focusing solely on monitoring the workspace.

7. ACKNOWLEDGEMENTS

This research is based upon work supported by the Federal District Research Support Foundation (FAP-DF).

8. REFERENCES

Campos, F.R., 2019. *Study of Teleoperation in Mining Applications (in Portuguese)*. Bachelor's thesis, Federal University of Ouro Preto (UFOP), Ouro Preto, Brasil.

Carrara, V., 2015. *Introduction to Industrial Robotics (in Portuguese)*. National Institute for Space Research (INPE) (in Portuguese), São Paulo, Brasil.

Forsslund, J., Yip, M. and Sallnäs, E.L., 2015. "Woodenhaptics: A starting kit for crafting force-reflecting spatial haptic devices". In *Proceedings of the 9th International Conference on Tangible, Embedded, and Embodied Interaction - TEI 2015*.

Goertz, R.C., Grimson, J.H. and Kohut, F.A., 1961. "Manipulator for slave robot". Patent, Registry number: US85074559A.

Khan, S., 2008. *Haptics and Virtual Reality*. Report, Department of Machine Design, KTH, Royal Institute of Technology, Stockholm, Sweden.

Martin, S. and Hillier, N., 2009. "Characterisation of the novint falcon haptic device for application as a robot manipulator". In *Proceedings of the Australasian Conference on Robotics and Automation - ACRA 2009*. Sydney, Australia.

Morrell, A.L., Morrell-Junior, A.C., Morrell, A.G., Mendes, J.M., Tustumi, F., de-Oliveira-e Silva, L.G. and Morrell, A., 2021. "The history of robotic surgery and its evolution: When illusion becomes reality". *Journal of the Brazilian College of Surgeons (in Portuguese)*.

Qian, S., Zi, B., Shang, W.W. and Xu, Q.S., 2018. "A review on cable-driven parallel robots". *Chinese Journal of Mechanical Engineering*, Vol. 31, p. 66.

Silva, J.M.F.d., 2014. *Study and Development of a Two-Degree-of-Freedom Haptic Device Based on Direct Current Actuators (in Portuguese)*. Master's thesis, University of Porto, Porto, Portugal.

9. RESPONSIBILITY NOTICE

The authors are solely responsible for the printed material included in this paper.